Indonesian Geotechnical Journal, April 2023, Vol 2 (1). Page 31 - 44
DOI: https://doi.org/10.56144/igj.v2i1.22
E-ISSN:2829-7520
https://indonesian-geotechnical-journal.org/index.php/JGI/issue/archive

Modelling Study of Pile Group Foundation by Including Lateral Load in Clay Soil

Muhammad Reza Imansyah[1*], Widjojo Adi Prakoso[2], Mulia Orientilize[3]
[1]Department of Civil and Environmental Engineering, Faculty of Engineering, Universitas Indonesia, Depok, Indonesia, 16424; muhammad.reza813@ui.ac.id
[2]Department of Civil and Environmental Engineering, Faculty of Engineering, Universitas Indonesia, Depok, Indonesia, 16424; wprakoso@eng.ui.ac.id
[3]Department of Civil and Environmental Engineering, Faculty of Engineering, Universitas Indonesia, Depok, Indonesia, 16424; mulia@eng.ui.ac.id
*Correspondence: muhammad.reza813@ui.ac.id

SUBMITTED 14 November 2022 **REVISED** 28 February 2023 **ACCEPTED** 1 March 2023

ABSTRACT Indonesia's geographical condition causes earthquakes to occur more frequently. This study aims to investigate pile group response under earthquake loading by performing pushover analysis. Since clay soil is dominant and widespread in Indonesia, the study focused on pile group embedded in single layer of clay. The undrained shear strength (S_u) parameters of the clay are varied from 20 kPa, to 100 kPa with 20 kPa intervals. The pile and soil were modelled by Beam-on-Nonlinear-Winkler-Foundation (BNWF), and the soil was presented as a series of Winkler springs using the nonlinear p-y method. The analysis was conducted with a finite element method (FEM) software, OpenSees. The pile was modelled as a fiber section, where the transversal and longitudinal reinforcement can be considered. The research found that the soil's S_u affects the ductility and formation of plastic hinge. Greater S_u resulted in higher ductility and occurrence of plastic hinge. Higher S_u was also found to increase the internal force experienced in the pile, as well as lead to higher group efficiency factor. There was no shear failure detected in the results, but bending failure happened at the lead pile in S_u 100 kPa. The overturning moment phenomenon occurred on the pile group in S_u 20 kPa and 100 kPa. For S_u = 20 kPa, this phenomenon is caused by the middle pile and rear pile, which did not have optimal performance. Bending failure at the lead pile led to the phenomenon in S_u 100 kPa.

KEYWORDS pile group foundation; undrained shear strength (S_u), pushover analysis.

1 INTRODUCTION

Data from the Meteorological, Climatological, and Geophysical Agency (Badan Meteorologi, Klimatologi, dan Geofisika; BMKG) reported that there were about 6000 times earthquakes that occurred in Indonesia in 2020. The data shows that the probability of an earthquake occurring in Indonesia is very high. Earthquake presents risks to people's lives, thus an in-depth study of the strength of structure required to survive an earthquake is needed. One of the essential components for earthquake-resistant building is its foundation. Modelling of the foundation's strength against earthquake can be simulated with lateral load.

Several studies have been carried out in the past to study the foundation performance against lateral load. Blanco et al. (2019) research proves that the larger lateral load will increase the strength and stiffness of the foundation. Nevertheless, the drastic increase makes the ultimate phase and the collapse of the foundation quicker. Ilyas et al. (2004) conducted centrifuge test of pile group embedded in clay subjected to lateral load. They also used nonlinear p-y method for their analysis. The experimental and analytical results show that the displacement in the lead piles is greater than piles from subsequent rows. Ilyas et al. (2004) also found that the pile group's efficiency decreases non-linearly with increasing lateral load. Lemnitzer et al. (2010) reported a full-scale cyclic lateral

load test on a 3 x 3 pile group. Different from Ilyas et al. (2004), the pile group efficiency decreases at low lateral displacement, but increases at higher lateral displacement.

Yuwono et al. (2020) conducted 3D numerical modelling using PLAXIS 3D to analyse behavior of piles embedded in clay subjected to lateral load. Pushover analysis was conducted to investigate the inelastic stage of the pile-soil system. The undrained shear strength (S_u) of soil was varied as 20 kPa, 40 kPa, 60 kPa, 80 kPa, and 100 kPa. The research found that at equal loading level, piles embedded in clay with lower undrained shear strength (S_u) experienced higher displacement. Although the software could model the soil in detail as a solid element, the pile can only be modelled as an elastoplastic beam element with an equivalent EA and EI. The reinforcement of the pile cannot be modelled. Thus, the inelastic behaviour that occurs in the pile cannot be properly captured. Hence, a comparative numerical study was carried out using Open System for Earthquake Engineering Simulation (OpenSees). With OpenSees, the pile can be modelled in detail. Pile can be modelled as fiber section, in which the prestressed pile with transverse reinforcement can be considered. In addition, longitudinal reinforcement can also be considered as pile confinement in each fiber section.

This research aims to study the pile-soil interaction with pushover analysis by identifying the internal forces, pile group efficiency factor, ductility, and occurrence of plastic hinges in the foundation. The pile group configuration was obtained from Yuwono et al. (2020). The pile-soil interaction was analyzed in Beam-on-Nonlinear-Winkler-Foundation (BNWF) model. As for the clay soil, it is modelled using nonlinear p-y method with P-Multiplier factor which differs in each row of pile.

2 METHODS AND MODELLING PROCESS

2.1 BNWF Modelling

The modelling process of BNWF is divided into foundation modelling and soil modelling. In foundation modelling step, the pile cap, axial load, and the pile itself are modelled. The pile cap was modelled as lumped mass and applied with axial load. The formula below is used to calculate the axial load for single pile:

$$P_{axial} = 0.1 \times f_c' \times A_g \quad (1)$$

where the value of f_c' (compressive strength of concrete after 28 days of curing) is 42 MPa and the value of A_g or pile's cross-section area is 250,000 mm^2 (the dimension of the pile is 500 x 500 mm square pile). This research used Yuwono et al. (2020) pile group configuration as shown in Figure 1. The axial load applied on the pile group is nine times of equation (1).

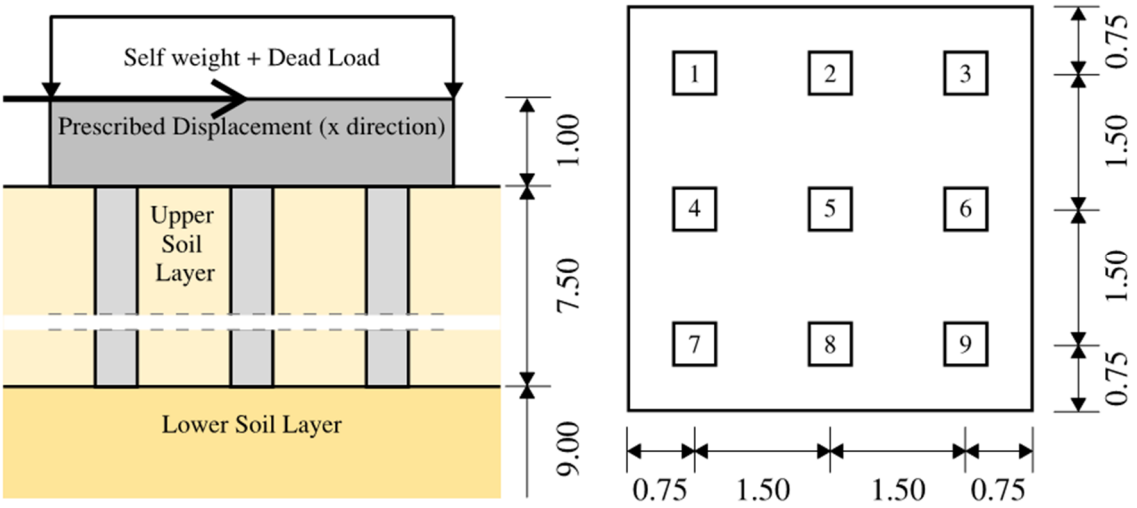

Figure 1. Dimensional attributes of modelled pile group (Redrawn from Yuwono et al., 2020), all units are in metres

This study used Kent & Park (1971) and Mander et al. (1988) formulas as input variables for concrete and steel reinforcement. All of the formulas are detailed in the appendix. In their studies, the confined concrete (inside the reinforcement) and unconfined concrete (outside the reinforcement) are modelled with different compressive strength (f_c'), so that the pile behaviour would be more realistic. The transversal reinforcement ratio (ρ_s) used is 0.01 (equation A.1 & A.6), and the yield strength of transversal reinforcement ($\boldsymbol{f_{yh}}$) is 4050 MPa. The longitudinal steel was modelled as prestressed steel PC Strand with 12.7 mm (0.5 inches) diameter. The yield strength of the longitudinal steel is 1488 MPa (80% of ultimate tensile strength), with jacking force of 1395 MPa (75% of ultimate tensile strength), and elasticity modulus is 200 GPa.

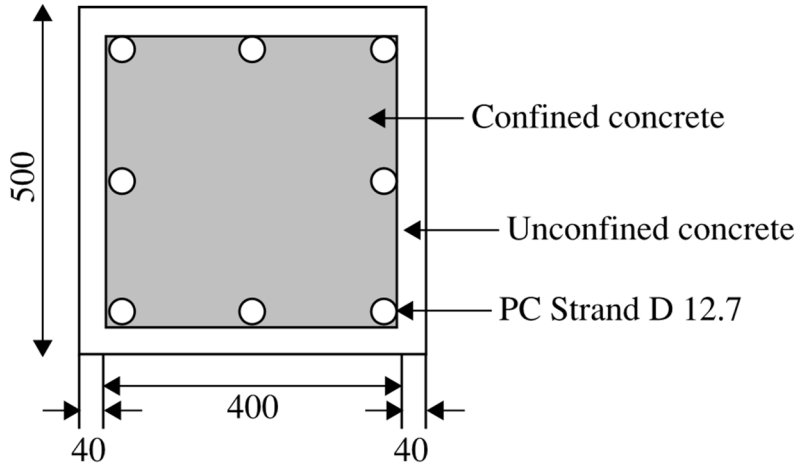

Figure 2. Cross-section of the pile

The Winkler springs were used to represent the soil. Nonlinear p-y methods were applied to the springs to find out the pile response under lateral load. For soft clay the simplified p-y method based on Matlock (1970) is used, while Reese & Welch (1972) p-y model was used for stiff clay. The p-y methods can evaluate the ultimate resistance (*Pu*), non-dimensional ultimate resistance coefficient (*Np*) and yield displacement (*dy*) using the following equations:

$$Pu = Np \times S_u \times D \tag{2}$$

$$Np = min\left[\left(\left(3 + \frac{\gamma_{eff}}{S_u}\right) + J \times \frac{z}{D}\right), 9\right] \tag{3}$$

$$dy = 2.5 \times \varepsilon_c \times D \tag{4}$$

This soil model's effective unit weight (γ_{eff}) is 7.19 kN/m^3 obtained from Budhu's (2010) reference for clay. For all of the S_u variations analyzed, the same γ_{eff} is used. This is because this research intends to isolate the impact of S_u only without the influence from other parameters. The *J* coefficient, which is the factor determined by Matlock (1970), equals to 0.5 for clay. The ground water level was placed on the ground surface of the soil. Furthermore, the strain coefficient (ε_c) is 0.02 for s_u 20 kPa, 0.01 for S_u 40 kPa, 0.006 for S_u 60 kPa and 80 kPa, and 0.005 for s_u 100 kPa. The *J* coefficient and ε_c values were obtained from Lemnitzer et al. (2013). Variable *z* stands for depth below ground surface in meters, and *D* is the pile diameter (the side for square pile) in meters.

In this BNWF model, the 7.5 m pile was discretized into 10 elements (11 nodes) with a distance of 0.75 m between each node. The length of plastic hinge was calculated using the Federal Highway Administration (2014) formula:

$$Lp = 0.1\,H + D \leq 1.5D \tag{5}$$

where *Lp* is the plastic hinge's length, *H* is the distance between the ground surface and to the contraflexure point, and *D* is the pile diameter (the side for square pile).

Every node had one spring. The weight of pile cap and axial load were applied in the center of the pile group. Likewise, the lateral load was also applied in the same position. Figure 3 illustrates the BNWF model with the external loads applied in this study.

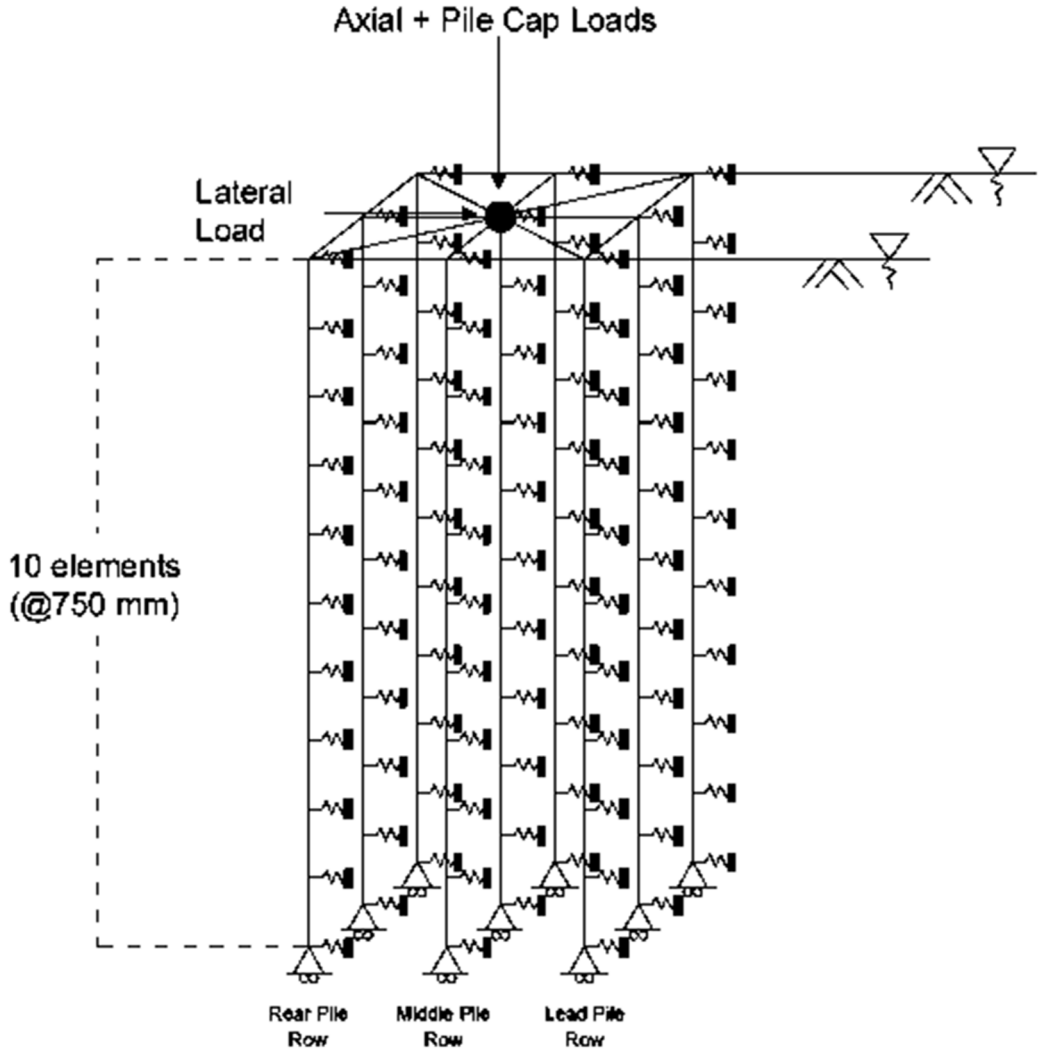

Figure 3. BNWF model

As shown in Figure 3, the lead pile row is the row of piles that is farthest from the direction of lateral load. So, the lead pile row carries the largest lateral load, followed by the middle pile row and the rear pile row.

2.2 Finite Element Method with OpenSees

Open System for Earthquake Engineering Simulation (OpenSees) is a software that analyzes pile-soil interaction by finite element method and nonlinear static analysis feature. OpenSees can model the movement and acceleration of soil. This analysis calculates the inelastic phase of the foundation structure. Therefore, the location of the structure's failure, such as the plastic hinge, can be detected.

In OpenSees, the foundation and soil components are modelled from geometry and material properties. OpenSees software models the pile with fiber section, which is capable of detailing the reinforcement of concrete, making the pushover analysis more realistic. Figure 4 displays the illustration of fiber section. Table 1 below shows the commands and details needed for the modelling process of this research.

Table 1. OpenSees commands for this research

Model		OpenSees Command	
Geometry	Node	ndm	3
		ndf	6
	Constraint	Single Point	Fix
	Element	Pile	dispBeamColumn
		Soil	zeroLength
		Pile Cap	ElasticBeamColumn
		Foundation Mass	Mass
Material	Uniaxial Material	Concrete	Concrete02
		Steel	Steel02
		Soil	PySimple1
Fiber Element	Section	Pile Section	patch quad
		Reinforcement	layer straight
Transformation	Element	Foundation	geomTransf PDelta
Pushover Analysis	Loads	Gravity	Linear
			Load
			Pattern Plain
		Pushover	Pattern
			DisplacementControl

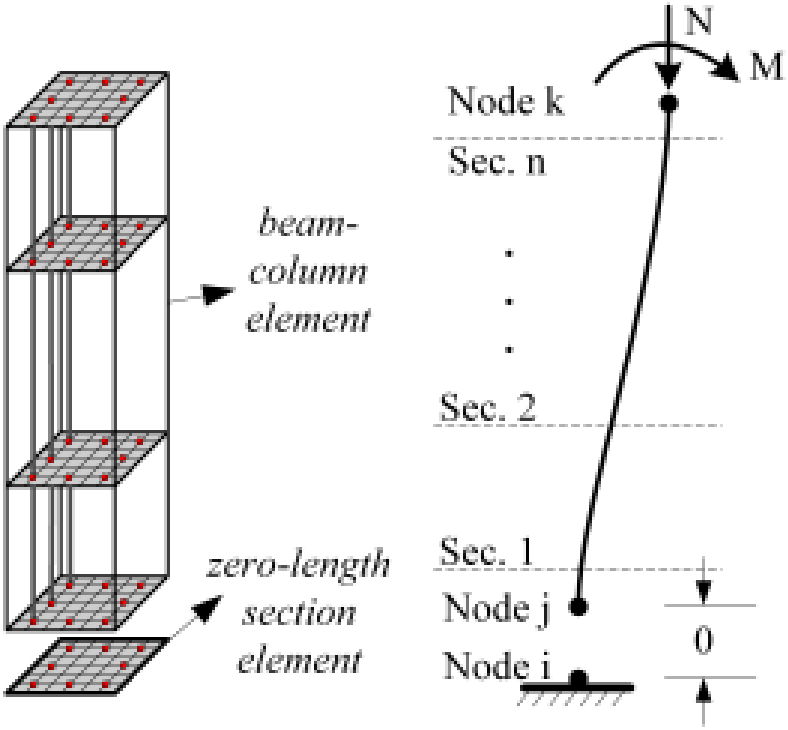

Figure 4. Fiber section illustration with some OpenSees commands (Mazzoni et al., 2006).

2.3 Comparison to Yuwono et al. (2020) Research

The pushover analysis results for single and group piles are compared to Yuwono et al. (2020) research. The first difference between these studies is that the previous research did not model the pile reinforcement. Yuwono et al.'s model was using beam elements with an elastoplastic constitutive model. The second difference was the P-Multiplier calibration. The 3D finite element model in Yuwono et al.'s research did not require the P-Multiplier factor in each row of piles, which is different from nonlinear model like this research. This study referred to the P-Multiplier values from Rollins et al. (1998), which are 0.6, 0.38, and 0.43 for the lead, middle, and rear pile, respectively.

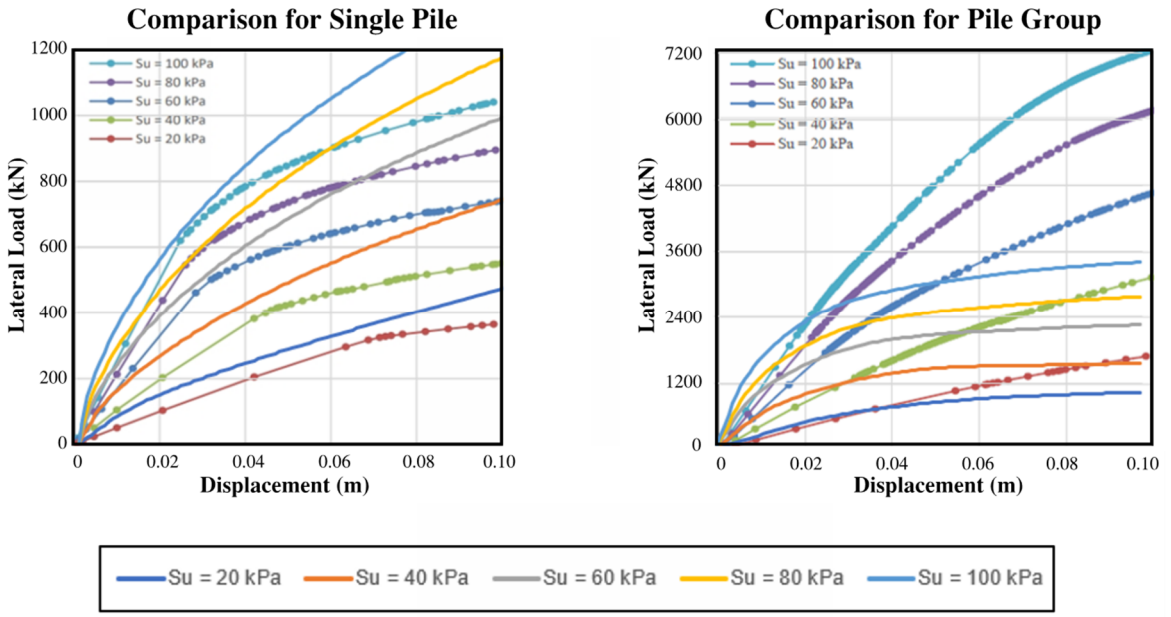

Figure 5. Comparison between Yuwono et al. (2020) and current research for single pile (left) and pile group (right) displacement response under lateral load. Yuwono et al. (2020) curve is the line with circular markers.

Figure 5 shows the comparison between Yuwono et al.'s results and current research. For single pile, the current research gives stiffer response than the previous results. On the other hand, for the pile group, opposite response can be observed. The pile group of Yuwono et al.'s research showed stiffer response. The difference was caused by the different characteristics between the elastoplastic and nonlinear p-y method. The nonlinear p-y method is better at capturing the yielding, plastic, and ultimate phases. The yielding phase can be graphically identified through the flattening of the pushover curve. In contrast, the elastoplastic method (Yuwono et al., 2020) does not have the flat phase after 0.1 m of displacement.

2.4 P-M Diagram

The P-M diagram is an interaction diagram between axial loads (P) and moment (M). The P-M diagram is influenced by longitudinal reinforcement, compressive strength of concrete, yielding strength of steel, and unit weight of concrete. The geometry of the pile, such as rectangular or cylindrical, also has an impact on this interaction between axial and bending moment loads.

This diagram visualizes the ability of a structure to resist the axial loads. If the point of interaction is outside of the diagram, it can be known that the structure is not able to resist the loads. In this study, the interaction was examined at axial loads from equation (1). Also, the P-M diagram in this study was obtained from SAP2000 software. The diagram was enlarged 1.25 times since there is an overstrength factor as an addition of maximum moment ability because of seismic loads (American Society of Civil Engineers, 2016).

2.5 Efficiency of Pile Group

The efficiency of pile group is represented by the ratio of the lateral response of the pile group to the total lateral response of a single pile foundation. This factor shows the quality performance of the pile group. The efficiency value depends on many factors, such as distance between each pile, lateral displacement, soil type, and P-Multiplier values. The efficiency factor of the pile group is calculated by the formula:

$$\eta = \frac{P_g}{N \times P_{sp}} \tag{6}$$

where η is the efficiency of pile group, P_g is the lateral response of pile group, N is the total number of piles in the pile group, and P_{sp} is the lateral response of the single pile. In this research, the efficiency of pile group was calculated for every lateral displacement analyzed.

2.6 Seismic Behavior

The seismic behavior is the structural behavior when the structure receives the seismic forces, which represents the earthquake condition. In this study, the behaviors analyzed were ductility and plastic hinge occurrences.

2.5.1. Ductility

Ductility is the structure's ability to deform in the post-elastic phase, which is caused by the cyclic earthquake force. A high value of ductility indicates better ability for the structure to resist earthquake load. There are many types of ductility, but this research only considers the displacement ductility. The formula of displacement ductility (μ) is:

$$\mu = \frac{\Delta u}{\Delta y} \tag{7}$$

Displacement ductility is the ratio of ultimate displacement (Δu) and yield displacement (Δy). Ultimate displacement is the displacement when the highest force is reached in pushover analysis. As for yield displacement, it is obtained when the moment reaches the yield moment of the structure.

2.5.2. Plastic Hinge

Plastic hinge forms at a point where the structure undergoes cracking and yielding with higher intensity, resulting in considerable displacement (Leslie, 2012). When plastic hinge occurs, the elastoplastic phase changes to the plastic phase of the structure. In general, plastic hinge would occur at the maximum bending moment of the structure. Usually, plastic hinge occurs in the pile head-pile cap joint connection (for the first plastic hinge) and the middle of the pile structure (for the second plastic hinge). Mathematically, a plastic hinge happens when the moment reaches the plastic moment of the structure. Figure 6 illustrates the process of the first (a to b) and secondary (b to c) plastic hinge.

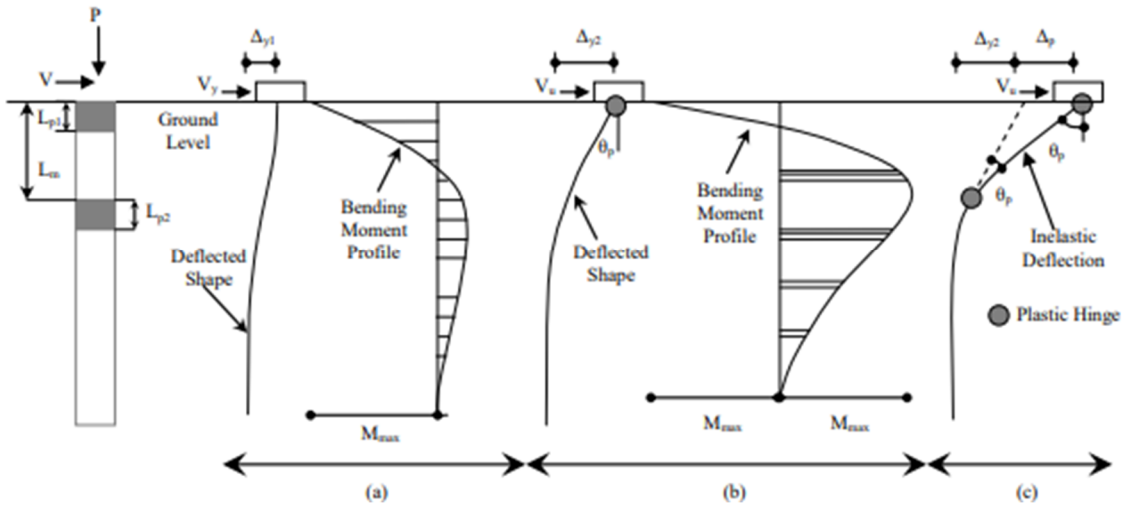

Figure 6. Development of Plastic hinge occurrence (Fanous et al., 2010)

3 RESULTS

Figure 7 shows the development of lateral load (shear force), bending moment and axial load with displacement for pile in lead pile row, middle pile row and rear pile row embedded in soil with different undrained shear strength. The results show that the magnitude of lateral load and bending

moment varies significantly with different S_u values. In contrast, there is no significant change in axial forces, except for S_u 20 kPa and 100 kPa.

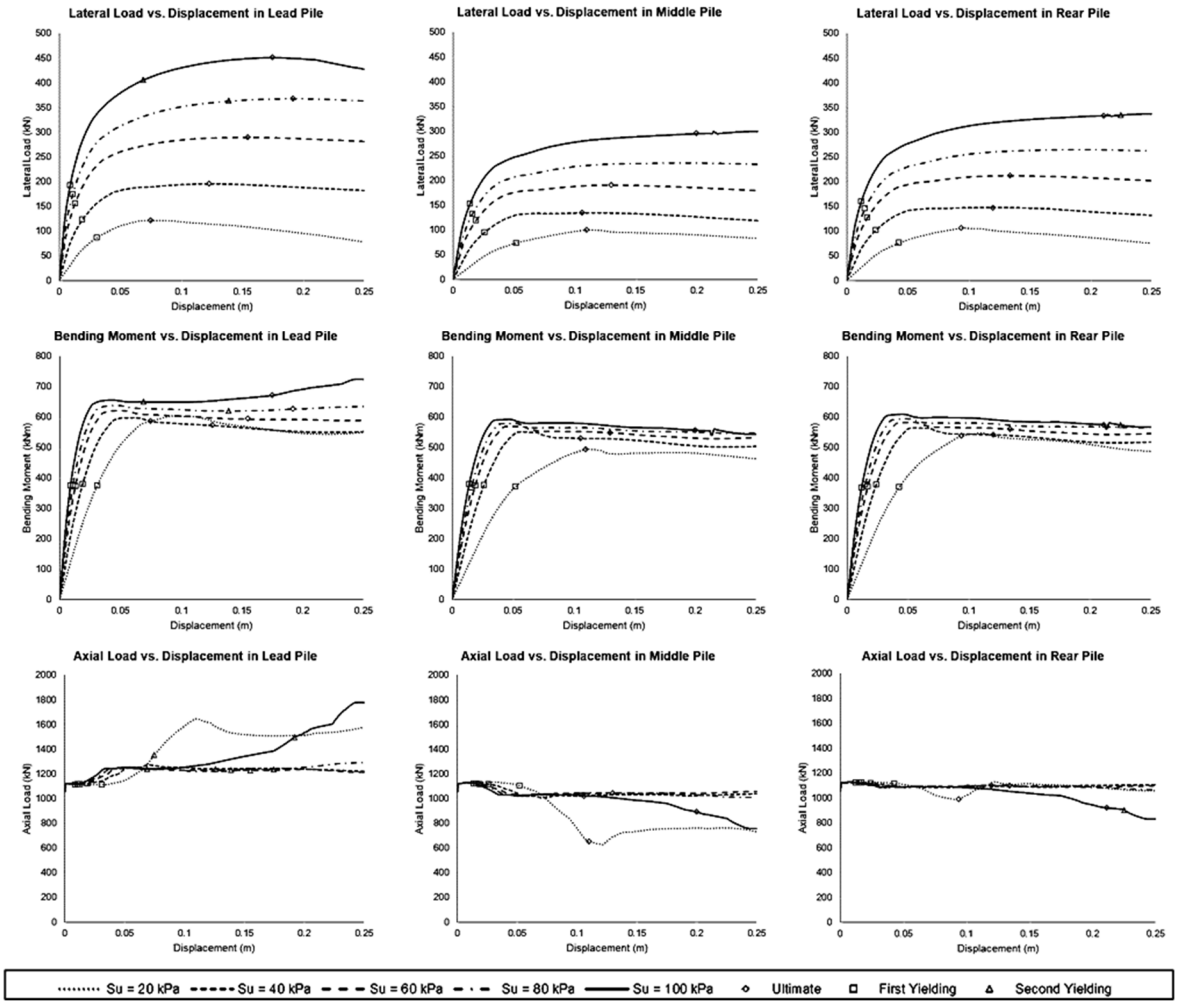

Figure 7. The internal forces (loads) versus displacement diagrams in all piles

The research continued by reviewing the P-M diagram. Figure 8 shows that only the lead pile in S_u 100 kPa has a P-M relationship outside the diagram.

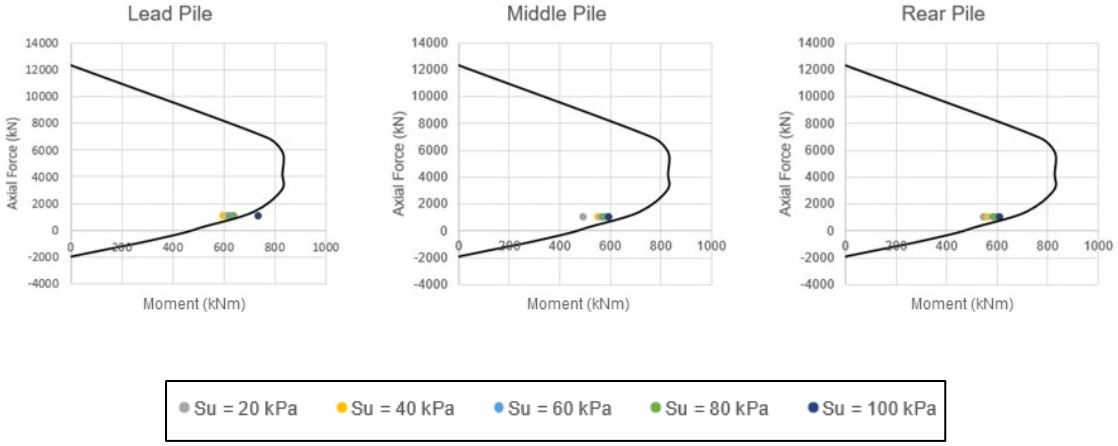

Figure 8. P-M diagram results

4 DISCUSSION

4.1 The Failure of The Pile

The internal forces of the piles at different pile row and at different displacement are shown in Figure 7. It can be seen that the undrained shear strength plays a big role in the development of shear force for all rows of pile. The largest shear force occurs in the lead pile for the pile group embedded in Su = 100 kPa. The shear force computed was about 450 kN, which is still lower than the maximum shear capacity of the pile = 906.76 kN (from SNI 2847:2019). None of the piles fail in shear mode. The checking of bending failure was based on P-M Diagram. Figure 8 shows that only the lead pile embedded in S_u 100 kPa has a P-M relationship outside of the envelope. This means that the lead pile embedded in S_u 100 kPa experienced bending failure. The greater the S_u, the stiffer the soil response, giving more resistance to the pile; leading to higher internal forces, hence higher possibility of structural failure.

There are several interesting observation in the internal forces vs displacement diagrams (Figure 7). The bending moment diagram for lead pile shows an anomaly in which the curve rises again at the end of the pushover process for S_u 20 kPa and 100 kPa. This data indicates the possibility of an overturning moment phenomenon in the pile group.

4.2 Overturning Moment Phenomenon

To study the overturning moment phenomenon, additional analysis on the axial forces diagrams was carried out. From the axial force vs. displacement diagrams in Figure 7, it can be seen that there is an increase in axial load for the lead pile and a decrease for the middle pile and rear pile for S_u 20 kPa and 100 kPa. This observation validates the occurrence of overturning moment in the pile group.

The occurrence of overturning moment was influenced by the magnitude of the P-Multiplier, which differed quite a lot between the lead piles compared to the other two rows. Therefore, the overturning moment did not occur at the midpoint of the pile group foundation (center of gravity), but rather, between the lead pile and the middle pile. The overturning moment is illustrated in Figure 9.

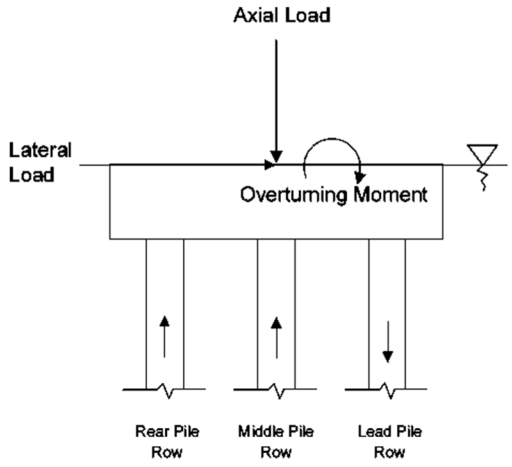

Figure 9. Overturning moment illustration

To further study the overturning moment, the pile deflection along the pile depth has to be investigated. The pile deflection profile at 0.25 m displacement is shown in Figure 10. For S_u 40 to 60 kPa, the pile deflection profile for lead pile, middle pile and rear pile are almost identical. Whereas there are differences in the pile deflection profile among the lead, middle and rear pile for S_u 20 kPa and 100 kPa. In S_u 20 kPa, the middle and rear pile's deflection was less than the lead pile. Hence, it can be deduced that the overturning moment occurred in S_u 20 kPa, which is the softest soil. The middle and rear piles were not optimal in supporting the structure of the pile group foundation, when the soil was too weak in resisting lateral load. For group pile in S_u 100 kPa, there was a nonlinear

deflection in the lead pile. The nonlinear deflection in lead pile is caused by structural failure, as shown in Figure 8. This affects the overall performance of the pile group. It can be concluded that the occurrence of an overturning moment also occurs for S_u 100 kPa, the stiffest soil.

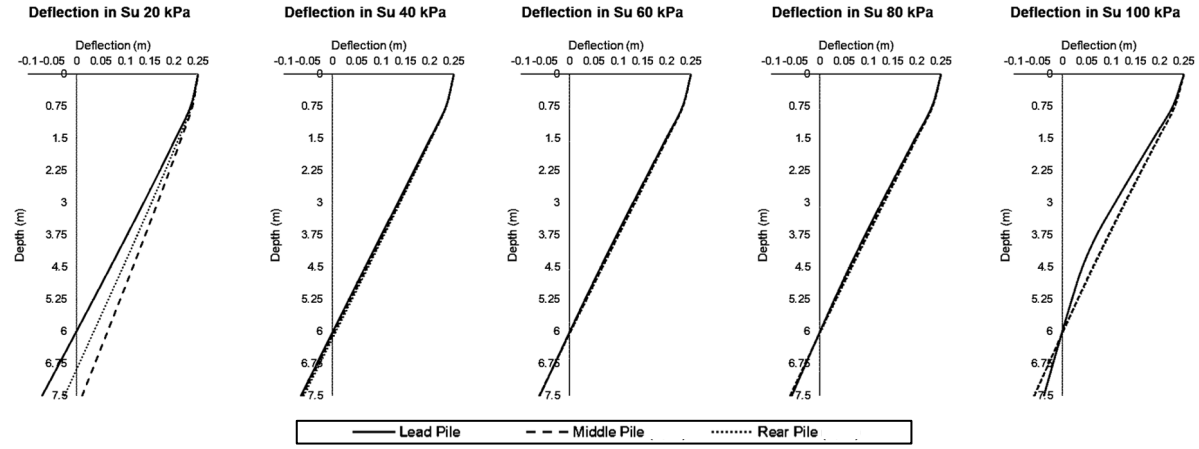

Figure 10. Piles deflection at 0.25 m pile cap displacement for every S_u variation.

4.3 Efficiency Factor of Pile Group

Based on equation (6), this research's efficiency factor is in the range of 0.1 – 0.46. Figure 11 displays the relationship between group efficiency factors and displacement.

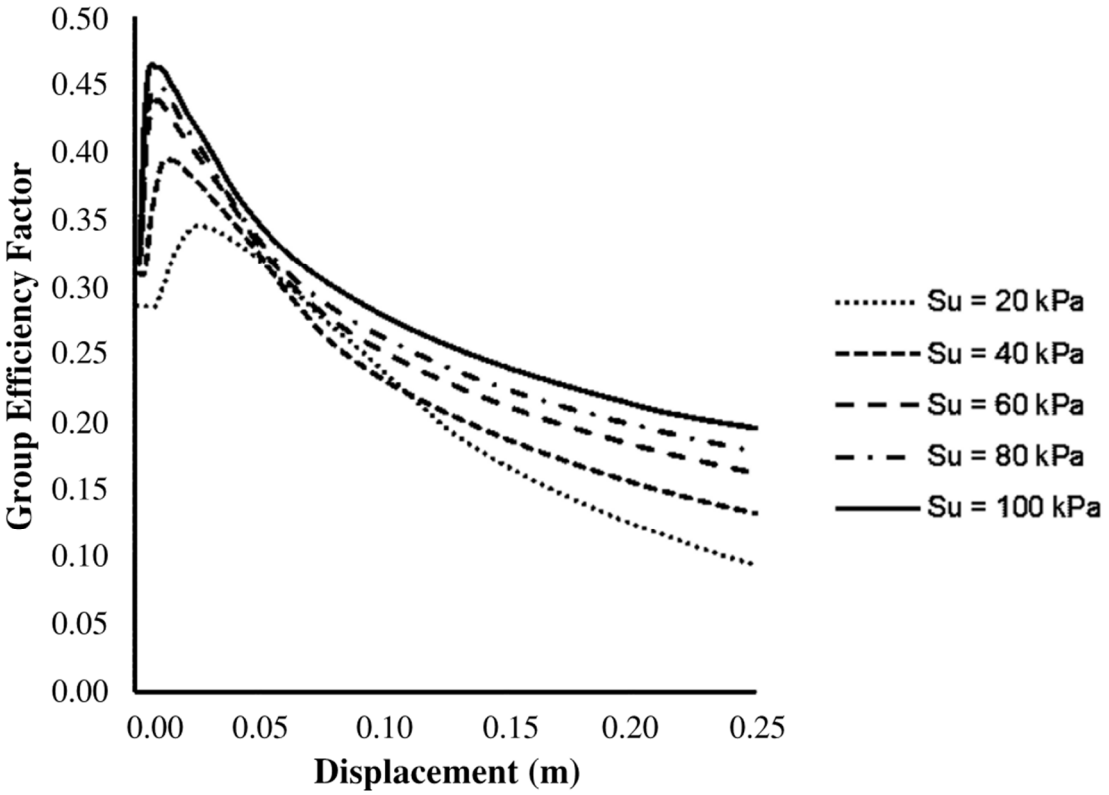

Figure 11. Relationship between group efficiency factor and lateral displacement.

Two observations can be seen From Figure 11. The first observation is that group efficiency factor reduces with reducing Su. The second observation is that the group efficiency factors increase at low displacement and reduces at higher displacement. It shows that the pile group performance would weaken when the pushover analysis is getting closer to the end. To maintain high group efficiency, it is crucial to prevent the pile group from reaching high lateral displacements.

The group efficiency from figure 11 is averaged for all the undrained shear strength analyzed. Figure 12 shows the averaged group efficiency compared to group efficiencies of 3x3 pile group embedded in clay obtained from existing literatures. It can be seen that the group efficiency obtained in this research is significantly smaller than previous research. It can be seen that the group efficiency factor does not show linear behaviour with pile group displacement for all research.

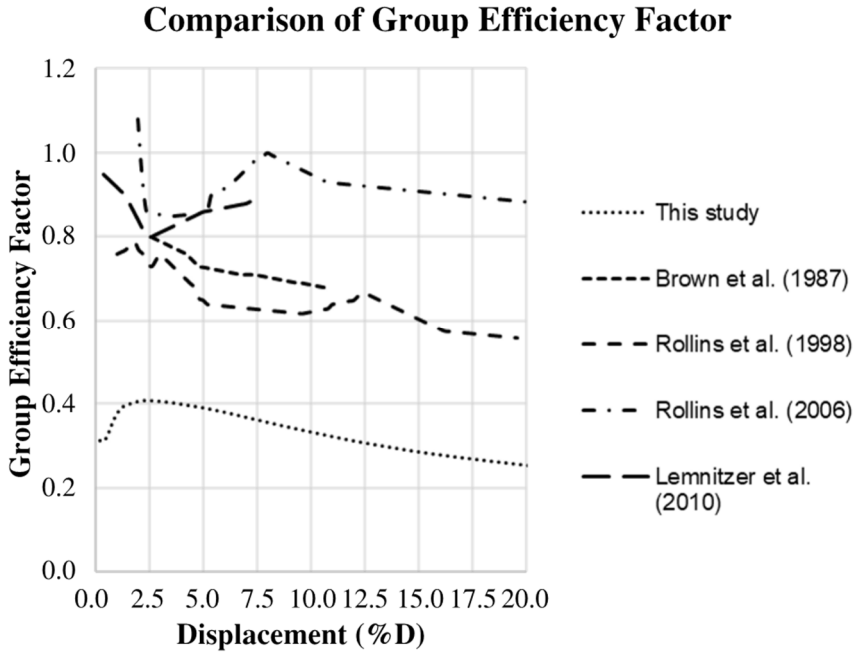

Figure 12. Validation of group efficiency factor with existing literatures.

4.4 Pile's Ductility

The larger the S_u, the lower the displacement required to reach yield. However, the larger the S_u, the higher the displacement to reach ultimate failure. The displacement values can be seen in Figure 7 (the yield displacement refers to the first yielding). Since ductility is the ratio of ultimate displacement to yield displacement, the greater the S_u value, the higher the ductility value. Hence, the greater the S_u value, the higher the resistance of pile structure against earthquake loads. Table 2 shows the ductility values obtained from this research.

In prestressed concrete, the yielding is enough to consider that the bending moment has reached the yielding moment (from SAP2000, it is at 367.624 kNm). Unlike in standard reinforcement steel, the yielding strain in prestressed steel cannot be obtained accurately.

Table 2. Pile's ductility in each S_u

Su (kPa)	Ductility		
	Lead Pile	Middle Pile	Rear Pile
20	2.419	2.115	2.186
40	6.474	4.077	5.000
60	11.923	6.842	7.882
80	17.454	-	-
100	19.444	14.286	17.583

From Table 2, it can be seen that S_u was not the only factor that affects the pile's ductility. The pile position also plays a role. This is due to the different P-Multiplier values that were assigned for different pile rows. The P-Multiplier values for lead, middle and rear piles are 0.6, 0.38 and 0.43 respectively. Following the assigned P-Multiplier values, the highest ductility is observed in lead pile, followed by rear pile, and finally the middle pile has the lowest ductility.

For this study, the ultimate displacement of the middle pile and rear pile with S_u 80 kPa was not obtained due to the drawbacks of the Steel02 material command on OpenSees in capturing the ultimate phase on prestressed concrete. It would be better to use ReinforcingSteel material command for the study of the pile's ductility.

4.5 The Occurrence of Plastic Hinge

Following Figure 6, plastic hinge first occurs at the joint connection between the pile cap and the pile head. As the pile experiences higher lateral displacement, a second plastic hinge occurs in the middle of the pile (around 3.5 m depth).

The research showed that plastic hinge only happened in the lead pile for S_u 80 kPa and 100 kPa. Only the first plastic hinge occurred, and there was no second plastic hinge in the model analyzed. The plastic hinge occurred in lower displacement for S_u 100 kPa than 80 kPa. It can be concluded that the greater the value of S_u, the occurrence of plastic hinge is more likely.

5 CONCLUSION

Pile group foundation modeling was analyzed by pushover analysis in BNWF. The model showed the pile-soil interaction in detail, with S_u as the parametric variable. It was found that soil with greater undrained shear strength leads to pile experiencing greater internal forces. The evaluation of internal forces found that none of the piles experiences shear failure, but there was a bending failure in the lead pile for S_u 100 kPa. The pile lateral response anomaly occurred in the softest (S_u 20 kPa) and stiffest (S_u 100 kPa) soil, where overturning moment happened. This phenomenon appeared because the role of each row of piles was too unbalanced for the pile group. The impact of S_u was on the group efficiency factor, where the greater S_u value tended to increase the efficiency of the pile group. The pile ductility increased as the S_u. The occurrence of plastic hinges was more likely and earlier in soil with higher S_u.

DISCLAIMER

The authors declare no conflict of interest.

AVAILABILITY OF DATA AND MATERIALS

All data are available from the author.

ACKNOWLEDGMENTS

The authors are very thankful to Mrs. Amelia Yuwono for the excellent research in foundation and earthquake engineering.

REFERENCES

American Society of Civil Engineers. 2016. *Minimum Design Loads for Buildings and Other Structures*. American Society of Civil Engineers.

Badan Standardisasi Nasional. 2019. "SNI 2847:2019."

Blanco, G., Ye, A., Wang, X., & Goicolea, J. M., 2019. Parametric Pushover Analysis on Elevated RC Pile-Cap Foundations for Bridges in Cohesionless Soils. *Journal of Bridge Engineering*, 24(1), pp. 04018104-1 to 04018104-18.

Budhu, M, 2010. *Soil Mechanics and Foundations*. New Jersey: John Wiley & Sons, Inc.

Fanous, A., Sritharan, S., Suleiman, M., Huang, J., & Arulmoli, K., 2010. Minimum Spiral Reinforcement Requirements and Lateral Displacement Limits for Prestressed Concrete Piles in High Seismic Regions.

Federal Highway Administration, 2014. *LRFD Seismic Analysis and Design of Bridges*. Washington,

D.C.: Federal Highway Administration.

Ilyas, T., Leung, C. F., Chow, Y. K., & Budi. S. S., 2004. Centrifuge Model Study of Laterally Loaded Pile Groups in Clay. *Journal of Geotechnical and Geoenvironmental Engineering* 130(3), pp. 274–283.

Kent, D. C., & Park, R., 1971. Flexural Members with Confined Concrete. *Journal of the Structural Division*, pp. 1969–90.

Leslie, R., 2012. The Pushover Analysis in Its Simplicity. *Civil Engineering &Construction Review,* 25, pp. 120-128.

Lemnitzer, A., Khalili-Tehrani, P., Ahlberg, E. R., Rha, C., Taciroglu, E., Wallace, J. W. & Stewart, J. P., 2010. Nonlinear Efficiency of Bored Pile Group under Lateral Loading. *Journal of Geotechnical and Environmental Engineering, ASCE*, 136(12), pp. 1673–1685.

Lemnitzer, A., Favaretti, C., Stuedlein, A., & Turner, J., 2013. P-Y Curve: Models. Available at: http://www.findapile.com/p-y-curves/p-y-curves-models [Accessed 14 November 2022].

Mander, J. B., Priestley, M. J. N., & Park, R., 1988. Theoretical Stress-Strain Model for Confined Concrete. *Journal Structure Engineering,* 114(8), pp. 1804–1206.

Matlock, H., 1970. Correlations for design of laterally loaded piles in soft clay. In *Proceedings of the Annual Offshore Technology Conference*. https://doi.org/10.4043/1204-ms

Mazzoni, S., McKenna, F., Scott, M. H., & Fenves, G. L., 2006. *OpenSees Command Language Manual*.

Reese, L. C., & Welch, R. C., 1972. *Lateral Load Behavior of Drilled Shafts*. ADSC International Association of Foundation Drilling.

Rollins, K. P., Peterson, K. T., & Weaver., T. J., 1998. Lateral Load Behavior of Full-Scale Pile Group in Clay. *ASCE Journal of Geotechnical and Geoenvironmental Engineering*, 124(6), pp. 467–478.

Yuwono, A., Prakoso, W. A., & Lase, Y., 2020. Preliminary 3D Numerical Pushover Analysis of Laterally Loaded Pile Groups. *IOP Conference Series: Materials Science and Engineering* 930(1).

APPENDIX

The equations below are from Mander et al. (1988):

$$\boldsymbol{k = 1 + \frac{\rho_s \times f_{yh}}{f'_c}} \quad \text{(A.1)}$$

$$\boldsymbol{f'_{cc} = k \times f'_c} \quad \text{(A.2)}$$

$$\boldsymbol{\varepsilon_{cc} = k \times \varepsilon_c} \quad \text{(A.3)}$$

where:

k = effectivity coefficient
ρ_s = transversal reinforcement ratio
$\boldsymbol{f_{yh}}$ = yield strength of transversal reinforcement (kPa)
$\boldsymbol{f'_c}$ = compressive strength of unconfined concrete (kPa)
$\boldsymbol{f'_{cc}}$ = compressive strength of confined concrete (kPa)
ε_c = strain of unconfined concrete
ε_{cc} = strain of confined concrete

Then, the equations below are from Kent & Park (1971). These equations are important to find the ultimate values of unconfined and confined concrete:

$$\boldsymbol{f'_{cu} = 0.4 \times f'_{cc}} \quad \text{(A.4)}$$

$$\boldsymbol{f'_u = 0.4 \times f'_c} \quad \text{(A.5)}$$

$$\boldsymbol{\varepsilon_{cu} = 0.004 + 0.9 \times \frac{\rho_s \times f_{yh}}{300}} \quad \text{(A.6)}$$

$$\boldsymbol{\varepsilon_u = 0.006} \quad \text{(A.7)}$$

where:

$\boldsymbol{f'_{cu}}$ = ultimate compressive strength of unconfined concrete (kPa)
$\boldsymbol{f'_u}$ = ultimate compressive strength of confined concrete (kPa)
$\boldsymbol{\varepsilon_{cu}}$ = ultimate strain of unconfined concrete
$\boldsymbol{\varepsilon_u}$ = ultimate strain of confined concrete

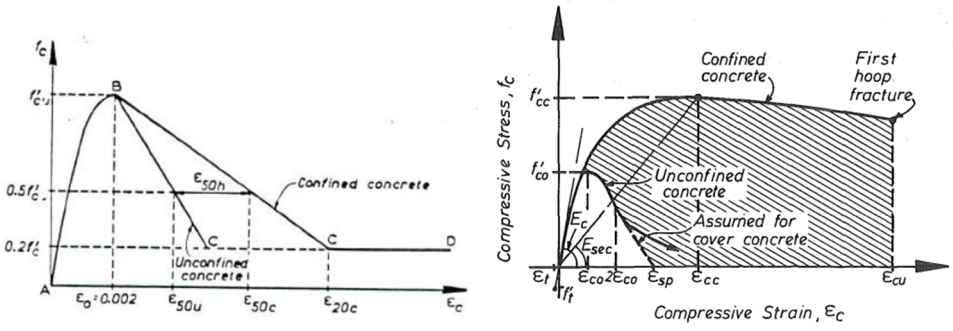

Figure A.1. Stress-strain model from Mander et al. (1988) (left) and Kent & Park (1971) (right).